Journal of Molecular Graphics and Modelling 57 (2015) 9–19

Contents lists available at ScienceDirect

Journal of Molecular Graphics and Modelling

journal homepage: www.elsevier.com/locate/JMGM

Theoretical studies on the deacylation step of acylated *Candida Antarctica* lipase B: Structural and reaction pathway analysis

Mohammad Sadegh Sadeghi Googheri [a,*], Mohammad Reza Housaindokht [a,b,*], Hassan Sabzyan [c]

[a] Biophysical Chemistry Laboratory, Department of Chemistry, Faculty of Science, Ferdowsi University of Mashhad, Mashhad, Iran
[b] Research and Technology Center of Biomolecules, Faculty of Science, Ferdowsi University of Mashhad, Mashhad, Iran
[c] Department of Chemistry, University of Isfahan, Isfahan, Iran

ARTICLE INFO

Article history:
Accepted 6 January 2015
Available online 14 January 2015

Keywords:
Enzymatic catalysis
DFT calculations
Energy profile
AIM investigation
Hydrogen bond interactions

ABSTRACT

The deacylation step of acylated *Candida Antarctica* lipase B, which was acylated with methylcaprylate (MEC) and acetylcholine (ACh), has been studied by using density functional theory method. Free energies of the entire reaction were calculated for enzyme deacylation by water and hydrogen peroxide that represented hydrolysis and perhydrolysis reactions, respectively. The calculations displayed that a stepwise mechanism there was with the enzyme–product complex being a deep minimum on the free energy surfaces of both of two reactions. The tetrahedral intermediate formation was the rate-determining step of all reactions, which needed 8.1 to 10.5 kcal mol^{-1} for activation in different reactions. In the second stage of the reaction, fewer free energy barriers, between 4.7 and 5.9 kcal mol^{-1}, were identified to enable the proton transfer from His224 to Ser105 and the breakdown of the tetrahedral intermediate. These calculated activation free energies approved theoretical possibility of both of two reactions for two substrates. Finally, an applied tool examined the interactions role in the stability and energy levels of different chemical species.

1. Introduction

In living creatures, enzymatic catalysts play essential roles in many of reactions. Chemical process that are catalyzed by enzymes commonly include complex mechanisms [1]. Therefore, characterization of their reaction mechanisms is an important and challengeable topic in biological chemistry [2,3]. Finding the reactions pathways has important implications in the design of mechanism-based inhibitors [4,5] and discovery of novel biocatalysts [6,7]. *Candida Antarctica* lipase B (CALB) as a functional, economic and common enzyme is considered significantly for mechanistic investigations [8–10]. Also, likeness of CALB active site and gorge structure as well as mechanism of action with acetylcholinesterase (AChE) puts it in the spotlight [11–13].

In our earlier article, the importance of study of acetylcholine (ACh) hydrolysis by *Candida Antarctica* lipase B (CALB) was explained in detail. As was mentioned, replacing the expensive acetylcholinesterase (AChE) enzyme with an economical enzyme, CALB, in lab studies can be useful [13]. It was shown the mechanism of CALB hydrolysis with its substrates, as AChE, is divided into two steps: acylation and deacylation. In the acylation step, formation of an acyl-enzyme (AE) occurs sequentially by a first noncovalent enzyme–substrate complex and a tetrahedral intermediate. In the deacylation step, hydrolysis continues with a second tetrahedral intermediate to give the enzyme-product complex (EP) [14–18]. Afterward the reaction mechanism of CALB acylation with methylcaprylate (MEC) and ACh was examined theoretically in that article, it was necessary that the second step of this reaction be studied and it be completed.

In the hydrolysis reaction, the deacylation step starts by proton transfer from the nucleophilic water to His224 and of an attack of the remaining hydroxyl on the ester carbonyl. It leads to form a tetrahedral intermediate (TI), which with a proton transfer from His224 to Ser105 and the breakdown of Ser105-COROR′ bond the enzyme–product complex is formed. The product of this hydrolysis reaction is a carboxylic acid. When the hydrogen peroxide there is in the environment can be entered in the reaction instead of water. In this case, the perhydrolysis reaction is occurred and the peroxy acid is formed (Fig. 1).

* Corresponding authors at: Biophysical Chemistry Laboratory, Department of Chemistry, Faculty of Science, Ferdowsi University of Mashhad, Mashhad, Iran. Tel.: +98 0 511 8796505; fax: +98 0 511 8796416.
E-mail address: sadeghi.mohammadsadegh@gmail.com (M.S. Sadeghi Googheri).

http://dx.doi.org/10.1016/j.jmgm.2015.01.003
1093-3263/

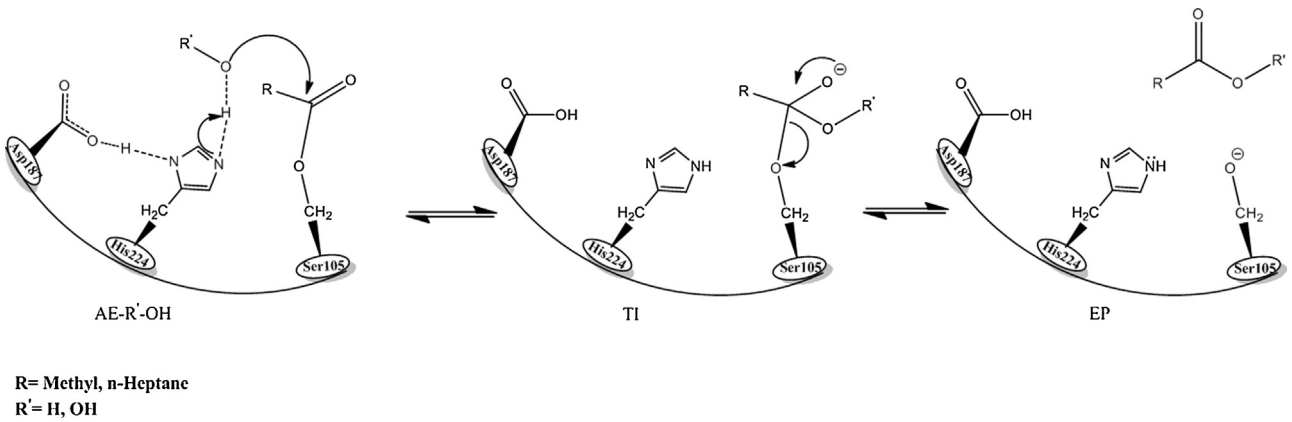

Fig. 1. Schematic representation of deacylation of acylated enzyme with water and hydrogen peroxide.

To complete the reaction and find out the deacylation step of it, we followed a similar pattern to previous work. We employed density functional theory (DFT) to study the reaction pathway of the AE deacylation. For the deacylation both water and hydrogen peroxide molecules were used and hydrolysis and perhydrolysis reactions were examined. As in previous the reaction mechanism of capryloyl–enzyme (Cap-E) deacylation, as the substrate of CALB that experimental results showed the hydrolysis of it, was studied and was used for comparison with acetyl-enzyme (Act-E) results.

The optimized AE structures were selected as the starting structures and a H_2O and H_2O_2 molecules were added to them for modeling the hydrolysis and perhydrolysis reactions. Other existent chemical species were designed from them and were optimized. We were using a two-step approach to reaction pathway analysis. At the first, optimization and frequency calculations were done at the low and executable level and then the single point computations were performed at higher level to improve results.

Further, for better understanding of effective limits in the energy order of reaction pathway the atoms in molecules (AIM) [19] theory was used. With this useful tool, we can discuss the nature of existent interactions in the active site region and their effects on the configuration stability and energy barriers.

2. Materials and methods

After the CALB acylation step was investigated for MEC and ACh substrates [13] to complete the reaction it was required that the deacylation step be studied. Our intent was to study both hydrolysis and perhydrolysis reactions. Therefore, the optimized AE structures of the acylation step were chosen to design the initial structures. For modeling the hydrolysis reaction one water molecule was added two these structures while the H_2O_2 molecule was applied for perhydrolysis reaction. It is mentioned that water and hydrogen peroxide molecules at first were optimized and then were added manually. These designed complexes, AE + H_2O and AE + H_2O_2, were considered as starter structures to deacylation stage. In these designed models, the acylated Ser105, His224, Asp187, Gln106 and Thr40 residues with H_2O and H_2O_2 molecules formed the QM subsystem (Fig. 2).

Here the Cap-E and Act-E complexes have 108 and 90 atoms in the hydrolysis model while in perhydrolysis model one hydrogen atom is added to each of them. It should be noted that the protonation state of His224 and Asp187 change during the reaction (see Fig. 3). DTF calculations were performed by applying the B3PW91 method in two steps for these structures.

The B3PW91 method uses two hybrid functional approximations, Becke three parameter [20] and Perdew-Wang91 [21], for estimation of the exchange–correlation energy functional. This offer an effective and exact method for calculation of non-local interactions as well as local interactions, which are efficient in the enzymatic reactions. Furthermore, this method has relatively good speed regarding other improved methods that is lead to decrease the cost of calculations.

In the first step, optimization was done at the best available and executable level of theory B3PW91/6-31G(d) followed by frequency calculations to confirm the nature of the stationary point [22]. Other chemical species containing tetrahedral intermediate (TI) and enzyme–product complex (EP) were created from this optimized construction and then optimization and frequency calculations of them were carried out at the same level of theory. Transition state structures, TS1 and TS2, were designed by gradually going from AE + HOR′ complex to TI and TI to EP, respectively. The OPT = TS keyword was used for optimization of these unstable structures at the same level of theory. Please note that to keep the residues place in protein structure the terminal atoms of them were frozen. To improve calculations of molecular geometries and properties, in second step, single point calculations were executed at B3PW91/6-311++G(d,p) [23] high-level of theory. The Conductor-like Polarizable Continuum Model (CPCM, solvent = water) was used for solvation effects [24,25]. All quantum mechanical calculations were performed by the Gaussian 09 [26] program packages.

Moreover, AIM theory was used for quantitative investigation of the prophesied important interactions for different structures in these reaction pathways. The single point calculations in the solvent environment approach were used to gain the correct wave function files for AIM analysis. All the QTAIM properties were calculated using the AIMQB program within the AIM Studio [27] suite, using the PROAIM basin integration method [28].

3. Results and discussions

3.1. Structural and energy analysis of reaction pathway

The catalytic pathway in which the acylated CALB was deacylated with H_2O and H_2O_2 is presented in Fig. 3. As can be seen each deacylation reaction has five chemical species including AE + R′OH complex, two TS structures, one TI, and EP complexes. The starting structures were AE + R′OH complexes, which were optimized at B3PW91/6-31G(d) level of theory followed by frequency calculations. TI and EP complexes structures were created based on these initial constructions and were optimized at the same level. No imaginary frequencies pointed out that we were in ground states, which are potential energy minimums in the potential energy surfaces (PES).

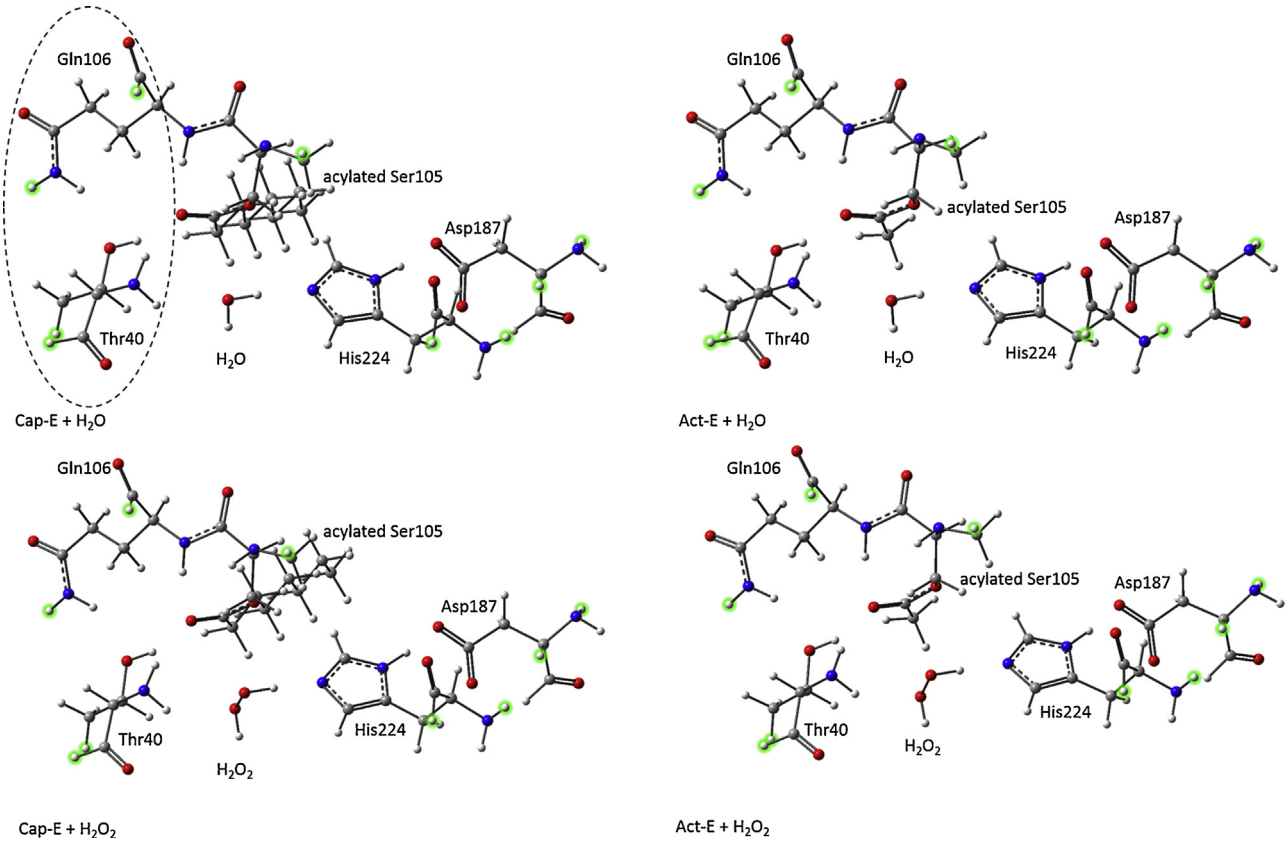

Fig. 2. Designed AE structures with H_2O and H_2O_2 molecules. These structures were considered as initial constructions for modeling the deacylation step. Fixed hydrogen atoms during the optimization are displayed as green halos. The oxyanion hole residues, Gln106 and Thr40, are specified with red oval. (For interpretation of the references to color in this figure legend, the reader is referred to the web version of this article.)

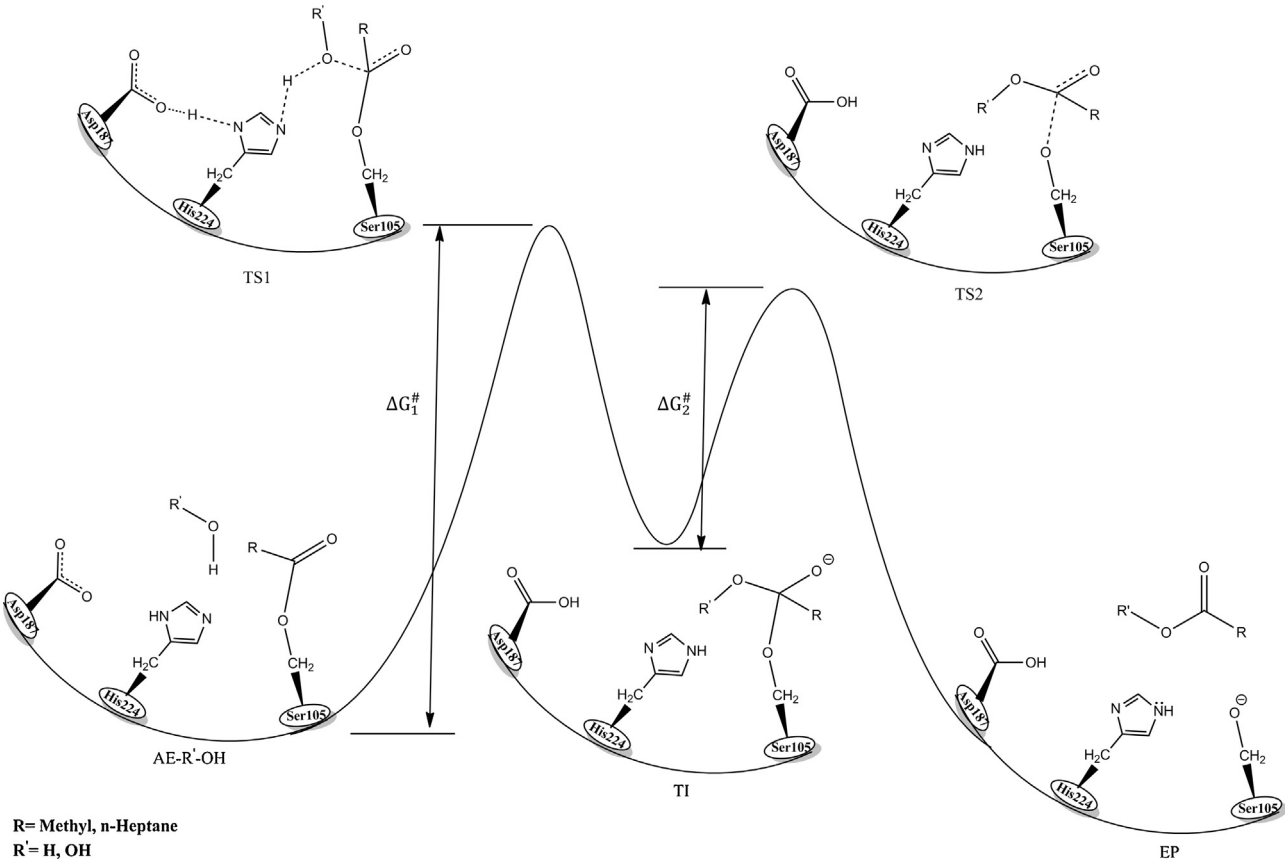

Fig. 3. Deacylation purposed mechanism of acylated enzyme. Five chemical species are determined from this reaction pathway.

Table 1
Topological parameters of different chemical species of deacylation reaction pathway. ρ_{BCP} and its Laplacian are in a.u. Related figures of this table are exhibited in Supporting information.

Chemical species	Involved bonds	Hydrolysis				Perhydrolysis			
		ρ_{BCP}		∇^2_ρ		ρ_{BCP}		∇^2_ρ	
		MEC	ACh	MEC	ACh	MEC	ACh	MEC	ACh
AE-R′-OH	Acyl – C = OLH – O – Thr40	0.033	0.033	0.116	0.115	0.031	0.031	0.110	0.110
	Acyl – C = O ··· H – N – Thr40	0.011	0.011	0.040	0.040	0.009	0.009	0.033	0.034
	Acyl – C = O ··· H – N – Gln106	0.018	0.018	0.064	0.063	0.019	0.020	0.068	0.068
	R′ – O – H ··· N – His224	0.039	0.039	0.096	0.096	0.056	0.057	0.102	0.102
TS1	Acyl – C = O ··· H – O – Thr40	0.036	0.037	0.123	0.124	0.035	0.037	0.118	0.118
	Acyl – C = O ··· H – N – Thr40	0.012	0.013	0.042	0.045	0.008	0.011	0.029	0.040
	Acyl – C = O ··· H – N – Gln106	0.017	0.018	0.056	0.058	0.019	0.019	0.062	0.065
	R′ – O – H ··· N – His224	0.063	0.065	0.096	0.097	0.065	0.066	0.138	0.136
	Acyl – C ··· OHR′	0.065	0.068	0.155	0.132	0.073	0.073	0.120	0.120
	C = O ··· H – O – OH	–	–	–	–	0.036	0.033	0.121	0.112
TI	Acyl – C = O ··· H – O – Thr40	0.050	0.050	0.138	0.135	0.048	0.048	0.136	0.136
	Acyl – C = O ··· H – N – Thr40	0.008	0.020	0.029	0.068	0.012	0.012	0.041	0.044
	Acyl – C = O ··· H – N – Gln106	0.023	0.024	0.073	0.075	0.020	0.020	0.066	0.066
	R′ – O ··· H – N – His224	0.033	0.032	0.106	0.105	0.034	0.033	0.110	0.107
	C = O ··· H – O – O	–	–	–	–	0.048	0.048	0.143	0.143
TS2	Acyl – C = O ··· H – O – Thr40	0.044	0.041	0.144	0.138	0.038	0.039	0.133	0.136
	Acyl – C = O ··· H – N – Thr40	0.020	0.020	0.069	0.072	0.017	0.017	0.061	0.058
	Acyl – C = O ··· H – N – Gln106	0.020	0.019	0.071	0.068	0.023	0.029	0.081	0.101
	Acyl – O – C ··· O – Ser106	0.079	0.079	0.134	0.135	0.078	0.077	0.139	0.147
	Ser105 – O ··· H – N – His224	0.088	0.088	0.145	0.144	0.087	0.086	0.143	0.149
EP	Gln – C = O ··· H – O – P	0.047	0.047	0.139	0.139	0.042	0.042	0.143	0.143
	Thr40 – O – H ··· O = C – P	0.038	0.038	0.135	0.135	0.027	0.027	0.096	0.099
	Ser105 – O – H ··· N – His224	0.044	0.044	0.099	0.099	0.046	0.046	0.102	0.102
	His224 – N – H ··· O – Asp187	0.058	0.059	0.131	0.132	0.068	0.067	0.137	0.137

Based on a proposed mechanism the first step in this reaction pathway is the water or H_2O_2 activation by the proton sharing with the histidine residue, followed a nucleophilic attack on the carbonyl group of the acyl group (Fig. 3). A gradually approach is adopted for designing the transition states from AE + R′OH structures. In this method, the hydrogen atom of the nucleophilic agent is transferred gradually to histidine residue, and simultaneously, the nucleophilic agent is shifted to the acyl group. This procedure is carried out by scanning the related geometric structural coordinates (Fig. 4a and b).

From TI to EP complex, the tetrahedral intermediate undergoes a rearrangement towards a more stable structure by the transition structure TS2 shown in Fig. 3. As it can be seen from this figure, the carbon–oxygen double bond begins to form and simultaneously, the single bond between the serine residue and carbonyl group of leaving group begins to break. The same technique as TS1 was used

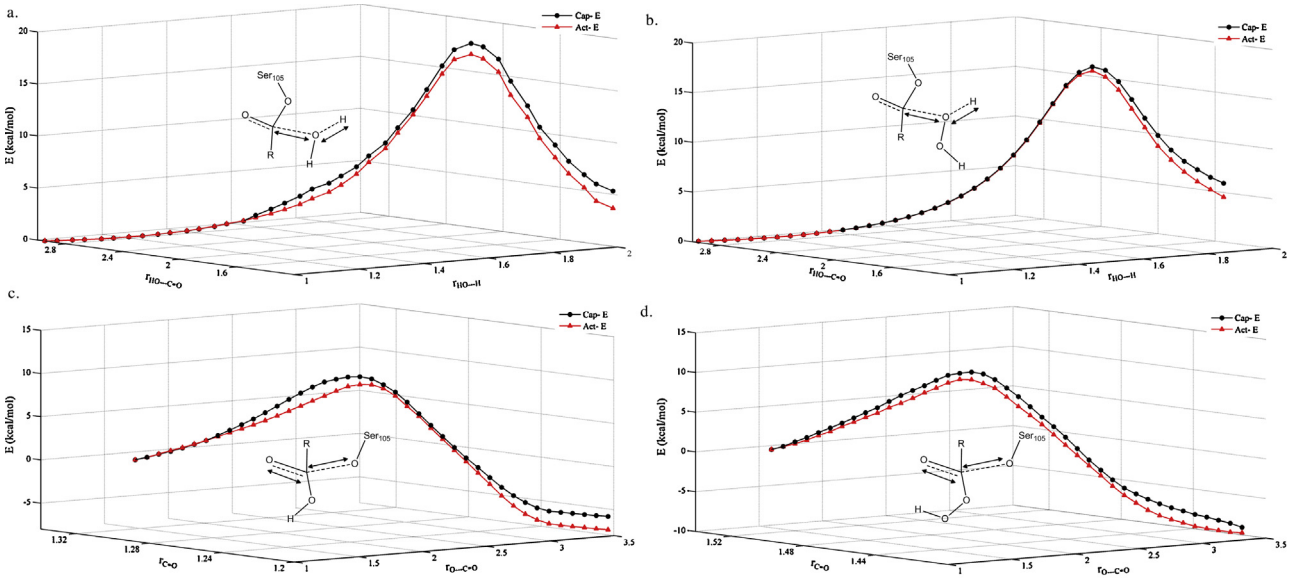

Fig. 4. Scanning scheme of passing from (a) TS1 of hydrolysis, (b) TS1 of perhydrolysis, (c) TS2 of hydrolysis and (d) TS2 of perhydrolysis for deacylation steps of two reactions. The maximums in the potential energy surfaces were chosen as TS constructions. The scanned distances are in Å.

Table 2
Relative energies (ΔE), relative energies with zero-point energy corrections ($\Delta(E+ZPE)$) and relative Gibbs free energies (ΔG) in kcal mol^{-1}, of chemical species in the optimization, B3PW91/6-31G(d), and single point calculation, B3PW91/6-311++G(d,p), levels of theories in the water environment.

Hydrolysis								
Chemical species	Cap-E				Act-E			
	6-31G(d)			6-311++G(d,p)	6-31G(d)			6-311++G(d,p)
	ΔE	$\Delta(E+ZPE)$	ΔG	ΔE	ΔE	$\Delta(E+ZPE)$	ΔG	ΔE
AE-H_2O	0.0	0.0	0.0	0.0	0.0	0.0	0.0	0.0
TS1	11.3	10.8	10.5	9.8	10.9	10.5	10.0	9.3
TI	6.9	6.5	6.3	6.0	7.3	7.0	6.8	6.4
TS2	12.5	11.7	12.2	11.4	13.6	12.7	12.4	12.4
EP	−7.3	−6.2	−8.2	−6.6	−6.9	−5.8	−6.2	−7.1
Perhydrolysis								
Chemical species	Cap-E				Act-E			
	6-31G(d)			6-311++G(d,p)	6-31G(d)			6-311++G(d,p)
	ΔE	$\Delta(E+ZPE)$	ΔG	ΔE	ΔE	$\Delta(E+ZPE)$	ΔG	ΔE
AE-H_2O_2	0.0	0.0	0.0	0.0	0.0	0.0	0.0	0.0
TS1	9.4	9.0	8.3	8.9	8.7	8.4	8.1	8.0
TI	4.9	4.3	4.4	4.5	4.4	4.7	4.4	5.2
TS2	9.7	10.2	9.5	9.7	9.3	10.3	9.1	9.7
EP	−8.3	−9.5	−8.8	−6.6	−9.6	−8.7	−7.1	−8.3

for scanning the pathway along these two coordinates to design TS2 structure, which their potential energy surfaces were displayed in Fig. 4c and d.

The maximums in the potential energy surfaces were chosen as the structures of transition states and were optimized to a transition state than a local minimum, using the Berny algorithm [29] at the same level of theory. Transition states were confirmed by imaginary frequencies in the vibrational frequency calculations. These observed frequencies located from 1581i to 1712i cm^{-1} for hydrolysis while they take the range 1684i to 1750i cm^{-1} in perhydrolysis reaction of two substrates.

The deacylation step starts by entering the nucleophilic agent into the active site region and formation of acyl-enzyme and nucleophilic agent (AE + R′OH) complex (see Fig. 3). The nucleophilic agent in hydrolysis reaction is the water whereas it is hydrogen peroxide for perhydrolysis reaction. Based on recommended mechanism the nucleophilic agent is activated by proton sharing with histidine residue. This significant activation can be inferred from

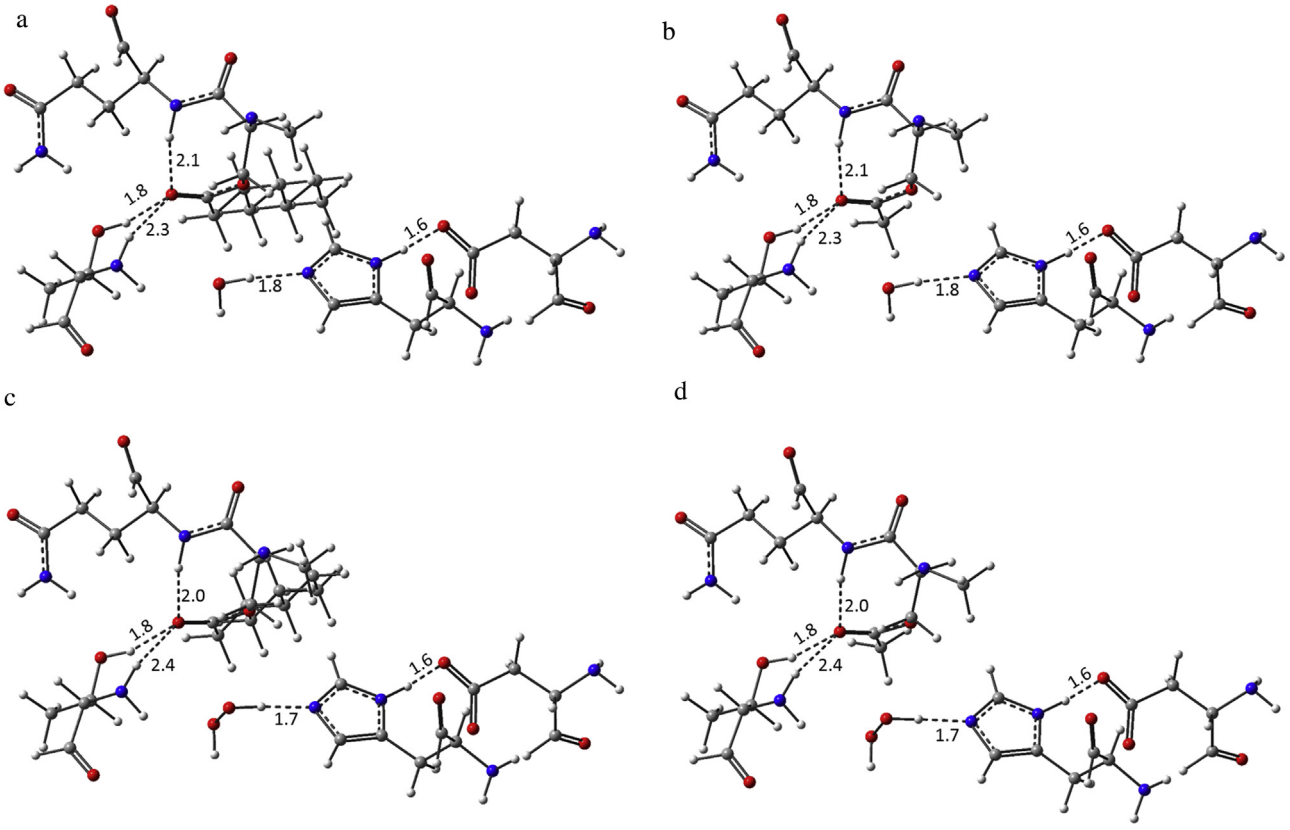

Fig. 5. Optimized structures of AE + HOR′ complexes for two reactions; (a) Cap-E···H_2O, (b) Act-E···H_2O, (c) Cap-E···H_2O_2 and (d) Act-E···H_2O_2. Proposed HBs and their bond lengths, in Å, are shown.

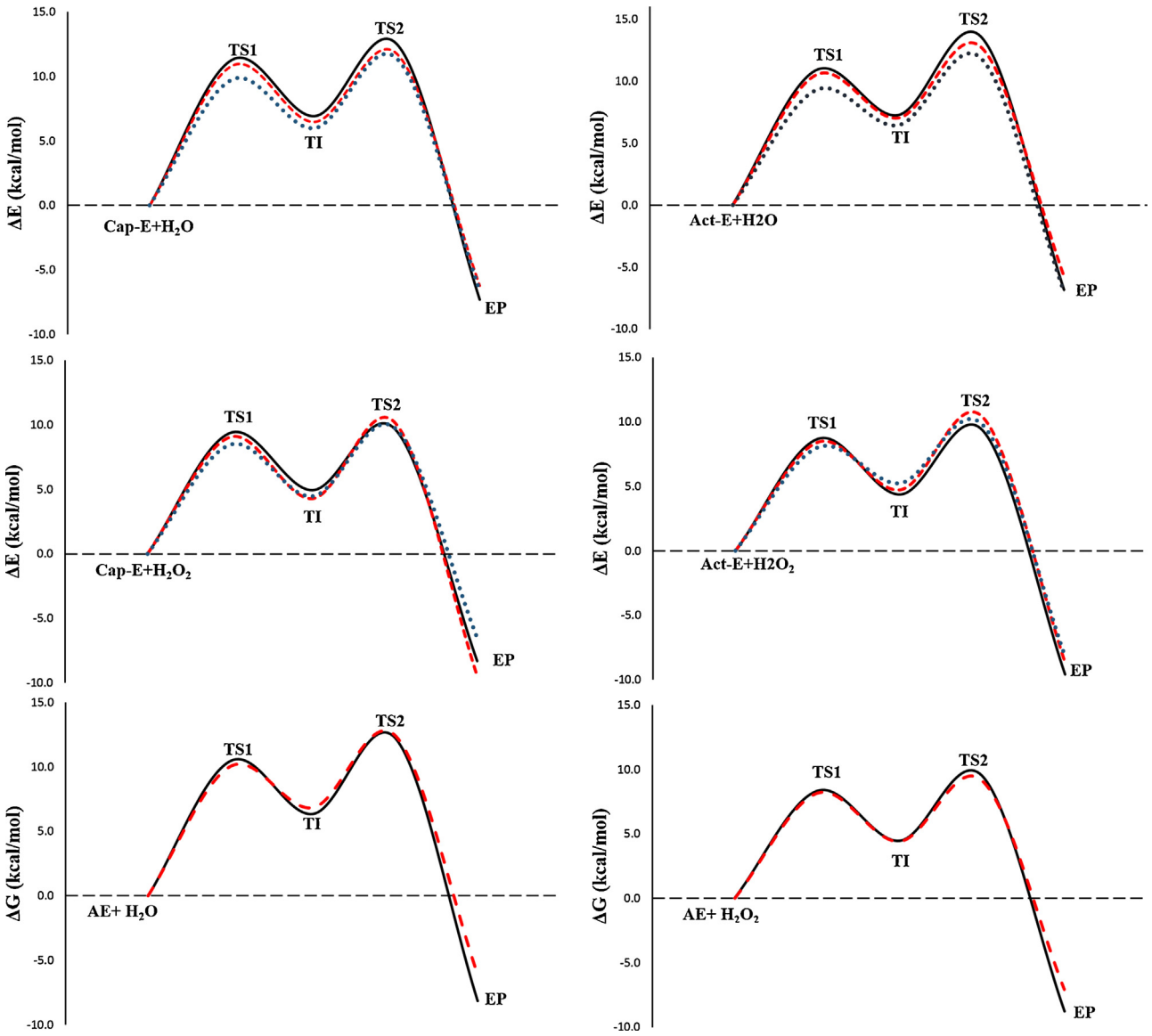

Fig. 6. Reaction pathways of deacylation steps of hydrolysis and perhydrolysis reactions based on energy and free energy viewpoints. In ΔE profiles, uncorrected pathways are black lines, pathways from zero point correction are red dashed lines and high level calculated energy profiles are in deep-blue dotted lines. In ΔG, the black and red dashed lines show the Cap-E and Act-E reaction pathways, respectively.

structural analysis of optimized structures in Fig. 5. Orientations of H_2O and H_2O_2 molecules with respect to histidine residue in both complexes and their distances in our optimized structures suggest hydrogen bonds (HBs) as an activating cause of nucleophilic agents.

Besides, it seems that the second cause in the reaction progress is activation of electrophile center, carbonyl group of linked acyl, which is done by oxyanion hole residues. This character of oxyanion hole in the activation is well represented in the optimized structures. The orientations of glutamine and threonine residues, as oxyanion hole, are such that the oxygen atom of acyl carbonyl group forms the HB with them. The hydrogen bonding network leads to lessen the charge density of carbonyl group and it becomes electrophile center (Fig. 5).

The AIM computable tool confirmed the existence of these HBs in these optimized structures. Based on similar pattern the electron density (ρ) and Laplacian of the electron density $\left(\nabla_\rho^2\right)$ values of bond critical point (BCP) were applied to quantitative judgment about HB formation. As previously noted, for a localized covalent bond the ρ and ∇_ρ^2 have positive and negative values while for a nonlocalized bond such as HB the ∇_ρ^2 value is positive. Topological parameters, $\left(\rho, \nabla_\rho^2\right)$ of bond critical point of AE + R′OH complexes are given in Table 1. Matching to these results a bond forms between the R′—OH and His224 residue while the C=O—HN-Thr40, C=O···HO—Thr40 and C=O···HN—Gln106 bonds are viewed in the oxyanion hole area. The watched ρ values vary between 0.010 and 0.057 a.u. whereas the ∇_ρ^2 values of bond critical points find in the 0.033–0.116 a.u. range. These detected electron density properties are as normal HB characters, which approve the hydrogen bonding interactions in the active site region.

Energy values of optimized structures of all species were extracted and the energies of the AE + R′OH complexes were selected as the references for the comparative analysis of our interest. The relative energies are reported in Table 2, and related potential energy surfaces are displayed in Fig. 6 to reaction pathway investigation.

To go from AE + R′OH complex to TI the reaction must pass through route TS1 construction, see Figs. Fig. 3 and 4a and b. Gained relative energies, Table 2, showed that both hydrolysis reactions wanted almost the same energy to pass from this energy barrier. In

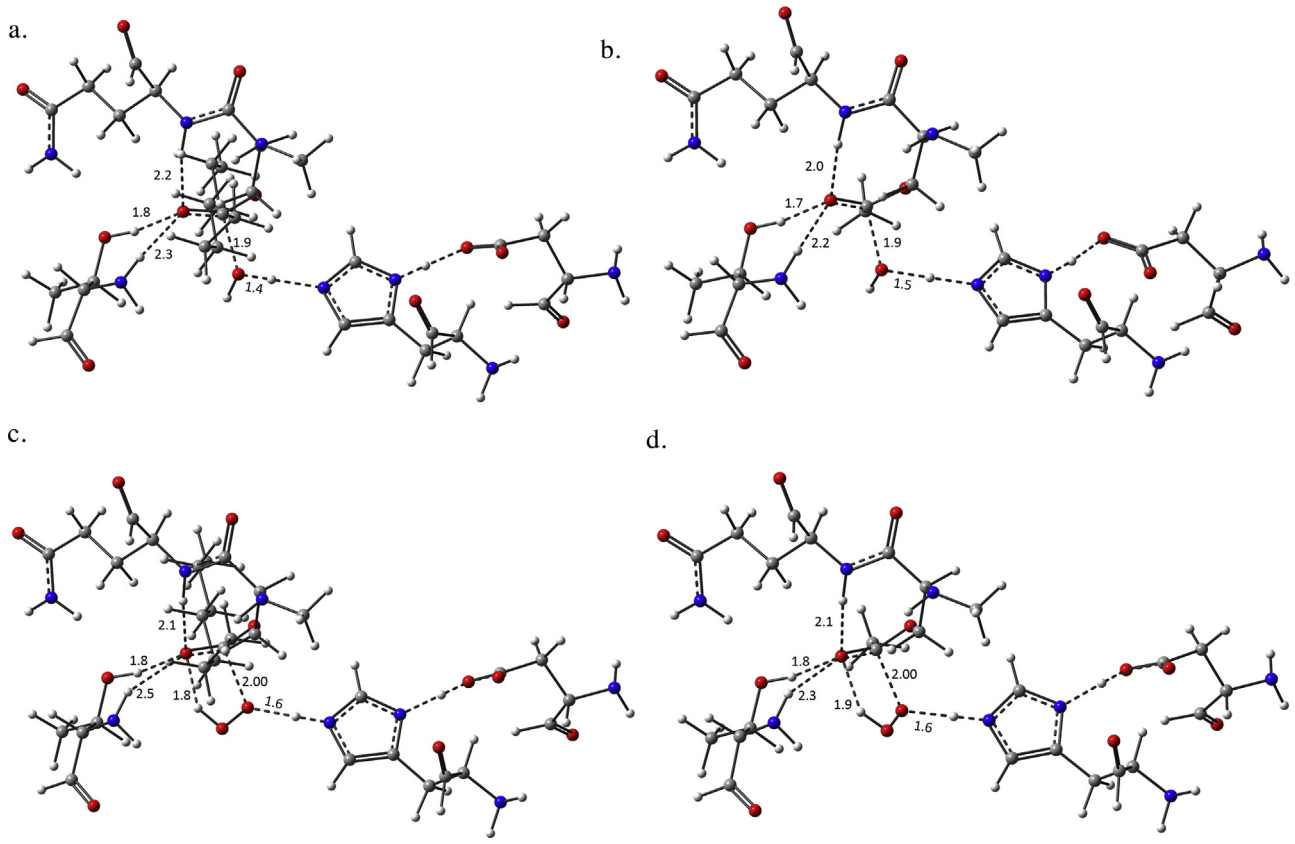

Fig. 7. Calculated TS1 structures for (a) hydrolysis of Cap-E, (b) hydrolysis of Act-E, (c) perhydrolysis of Cap-E and (d) perhydrolysis of Act-E. Effective HBs and their bond lengths, in Å, are shown.

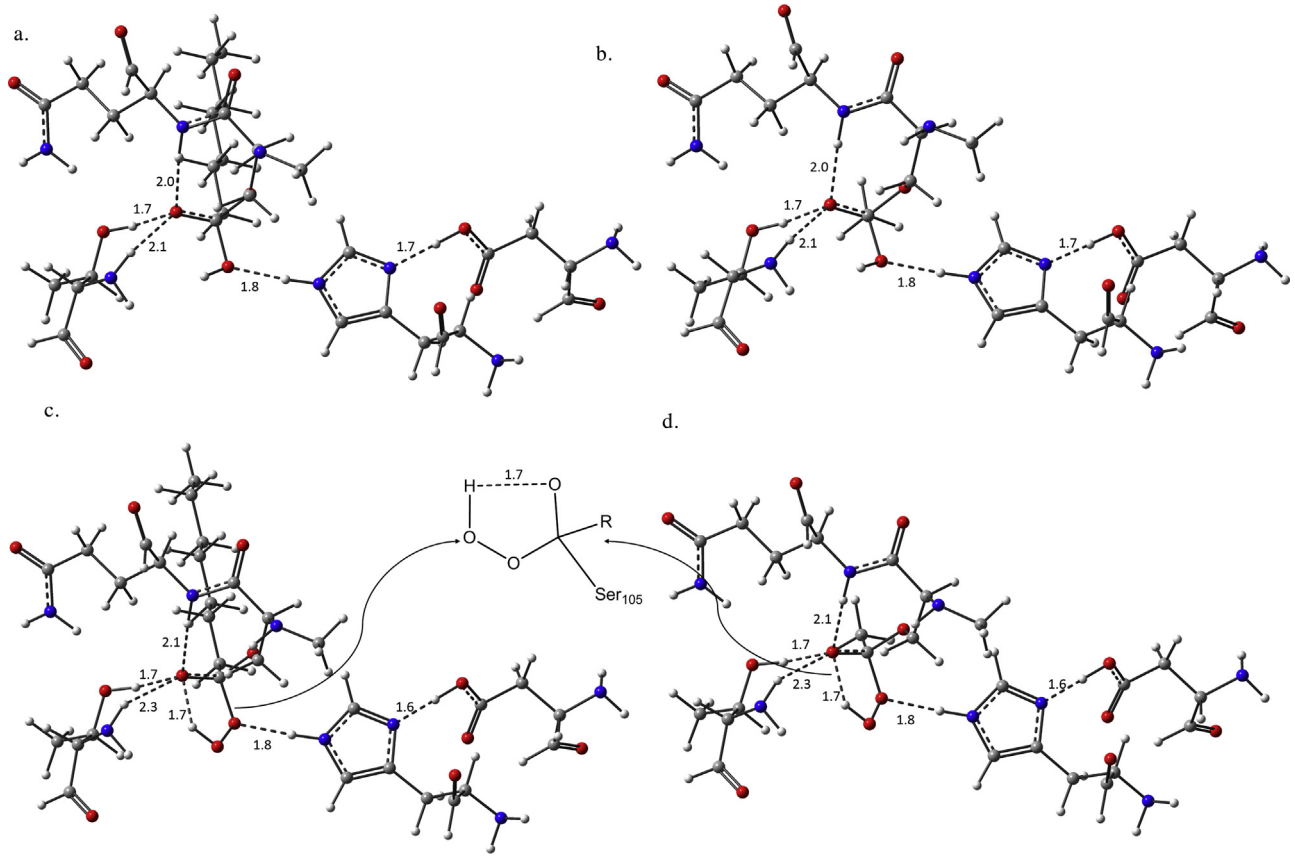

Fig. 8. Calculated TI structures for (a) hydrolysis of Cap-E, (b) hydrolysis of Act-E, (c) perhydrolysis of Cap-E and (d) perhydrolysis of Act-E. Effective HBs and their bond lengths, in Å, are shown.

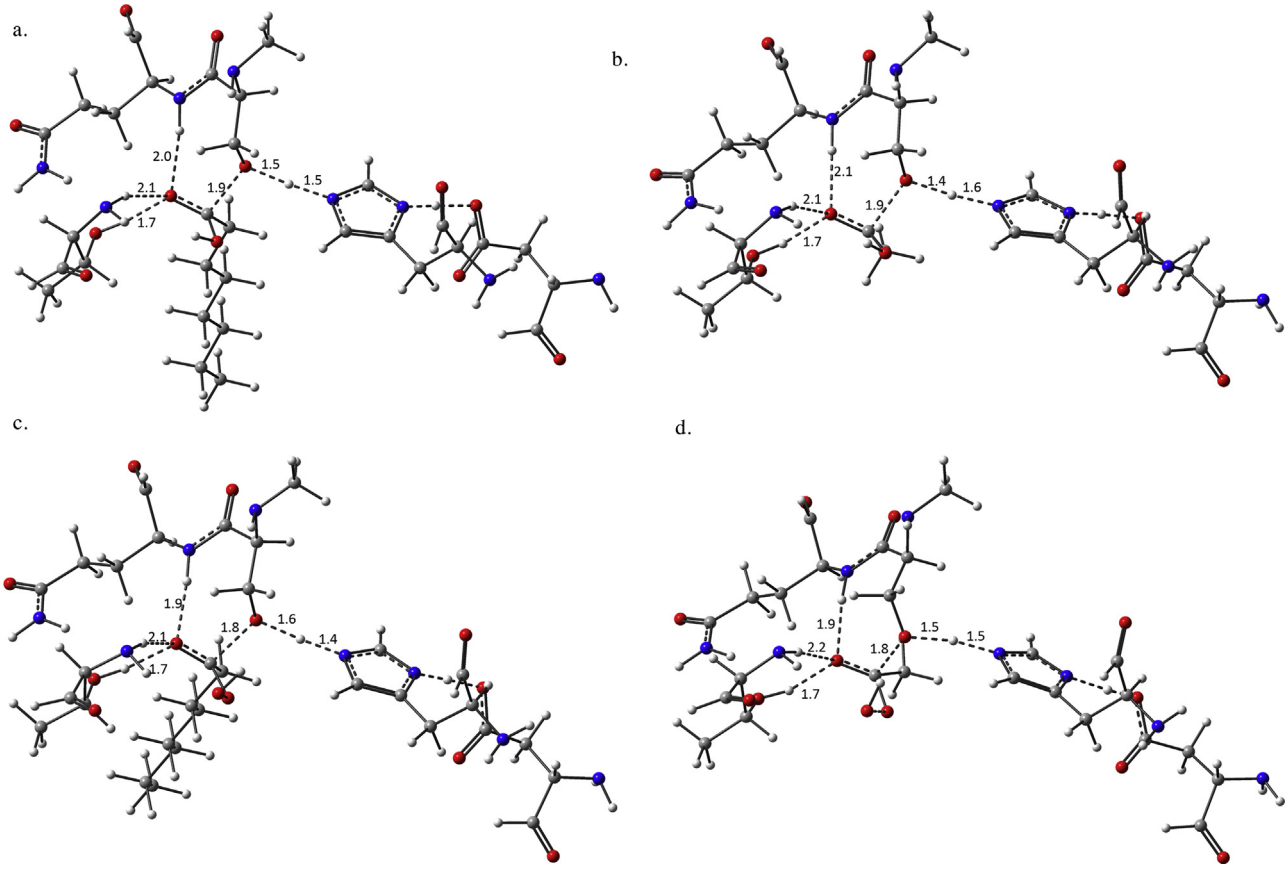

Fig. 9. Calculated TS2 structures for (a) hydrolysis of Cap-E, (b) hydrolysis of Act-E, (c) perhydrolysis of Cap-E and (d) perhydrolysis of Act-E. Effective HBs and their bond lengths, in Å, are shown.

other words, activation energies of two reactions are nearly identical that are clear from Fig. 6.

It seems that this energy likeness comes from structural likeness of transition state constructions. Detailed structural analysis of optimized TSs of hydrolysis reactions shows that position and numbers of involved bonds in the transition states are about similar (Fig. 7a and b). As is clear, position and type of predicted HBs are similar for two substrates. In addition, almost identical HBs power can be observed from topological parameters of bond critical points, Table 1, that imply same interactions for these TSs structures. This means that in this stage of hydrolysis reaction the TS geometry and its stabilizing reasons are identical for two substrates, which leads to likeness of activation energies for them. However, the steric hindrances are less for acetyl group but this cause does not have significant effect on the energy barriers.

The same behavior is observed for perhydrolysis reactions. Here also passing from TS1 maximum for two substrates needs nearly identical energy, which comes from the same causes. Structural analysis of optimized transition states of perhydrolysis reactions, Fig. 7c and d, confirms this suggestion. Likenesses of positions and numbers of HBs in these optimized structures make energy barriers almost identical. The same results are obtained from comparison of HBs power by topological parameters (Table 1). BCP densities of HBs for two TS1 structures are similar, which means that the HBs power are almost identical.

Although the first activation energies of each reaction are similar, there is a significant difference between the first energy barriers of hydrolysis and perhydrolysis reactions. Our energy calculations point out that the perhydrolysis reaction of two substrates needs fewer energy than hydrolysis reaction to pass from TS1 peak. This energy dissimilarity changes between 1.3 to 2.2 kcal mol^{-1} at different calculation levels. We guess that this decrease in energy barriers arises from forming a new HB. Our results show a new HB as HO—O—H···O=CR—Ser105, which does not viewed in the TS1s of hydrolysis reaction (see Fig. 7 and Table 1).

A similar behavior between free energy barriers can be detected from Table 2 and Fig. 6. As is obvious both substrates want the same free energy barriers to pass from TS1 in hydrolysis reaction. Equally, in perhydrolysis reaction the TS1 maximums are left behind with the identical free energies for two substrates. Except that, here the fewer free energies from 1.9 to 2.2 kcal mol^{-1} are needed. As explained before, these manners arise from arrangement of optimized transition state structures.

As is mentioned when the nucleophilic attack of R′—OH occurs the AE + R′OH complex by passing from TS1 structure converts to the stable tetrahedral intermediate. In this special structure, the R′—O group bonds to carbon atom of acyl carbonyl group and carbon–oxygen double bond becomes single. This leads to formation a tetrahedral structure with a central carbon atom, which its oxygen atom carries a negative charge. Here the role of oxyanion hole becomes more mentioned in this reaction by stabilizing this tetrahedral structure. Hydrogen bonding formation between the side chains of Thr40 and Gln106 residues with negative oxygen atom were distinguished from optimized structures. Calculated geometry of oxyanion hole residues with respect to tetrahedral structure, see Fig. 8, are in such a way that the HBs could be formed. These HBs form bond critical points between involved atoms, which come from electron transfer between their orbitals (Table 1).

This intermediate structure has more energy than AE + R′OH complex in the potential energy surface. Based on our results in

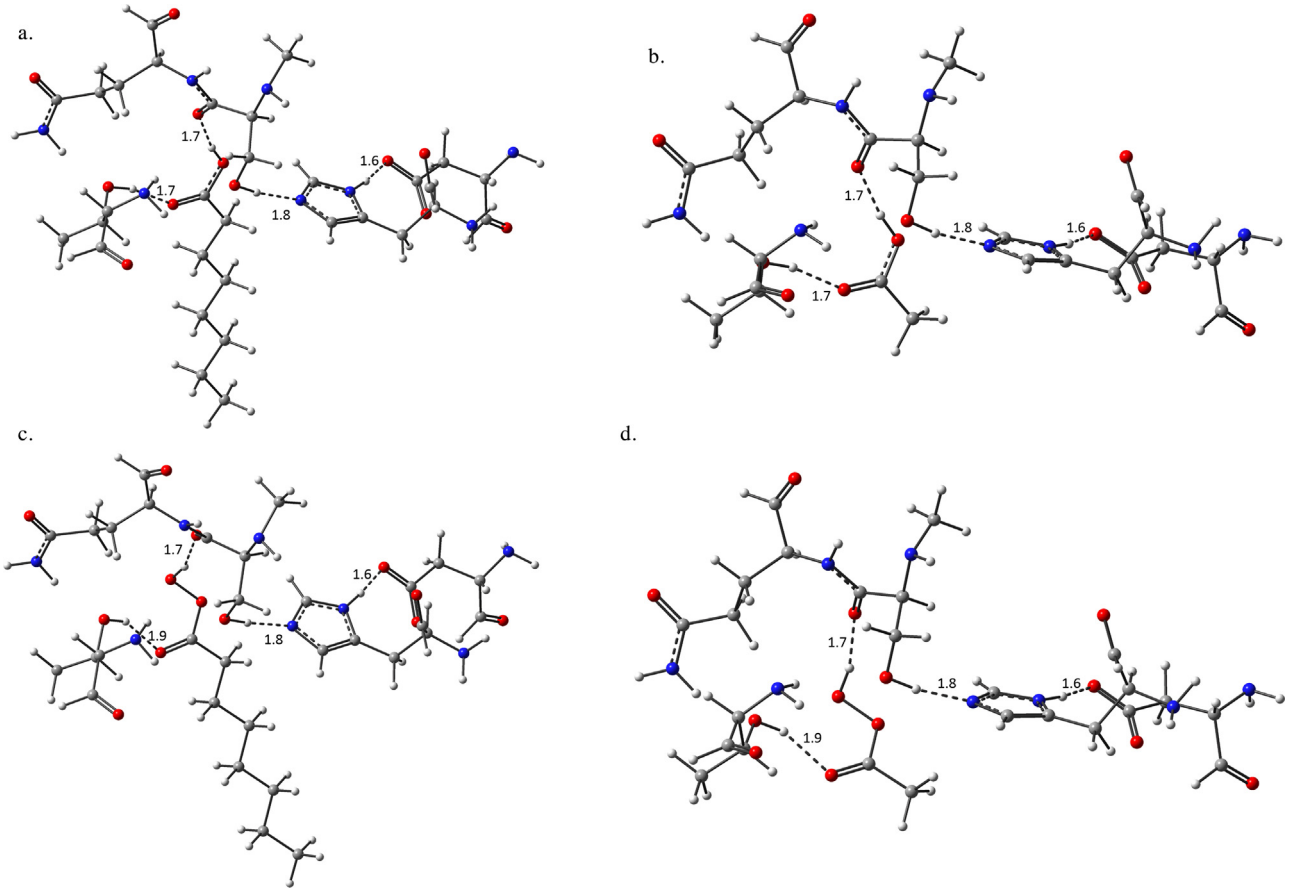

Fig. 10. Calculated EP structures for (a) hydrolysis of Cap-E, (b) hydrolysis of Act-E, (c) perhydrolysis of Cap-E and (d) perhydrolysis of Act-E. Effective HBs and their bond lengths, in Å, are shown.

hydrolysis reactions, this instability is between 6.0 to 7.3 kcal mol^{-1} while it changes from 4.3 to 5.2 kcal mol^{-1} in perhydrolysis reactions at different computational levels (see Table 2 and Fig. 6). Cause of this difference between hydrolysis and perhydrolysis reactions can be concluded from calculated TI structures. In the TIs of perhydrolysis reaction an intermolecular HB is formed, which does not detected in the TIs of hydrolysis reaction (see Fig. 8). This additional HB that can be observed from AIM results, Table 1, increases the stability of TI and decreases its energy level.

The second transition state construction is formed in the pathway of TI to EP, which its optimized structures of two reactions are shown in Fig. 9. To design the TS2 structures two parameters including the C—O bond length of carbonyl group, r_{C-O}, and the distance between carbon of carbonyl and oxygen of Ser105 residue, $r_{O-C\cdots O-Ser105}$, were scanned concurrently (Fig. 4c and d). Bond length analysis shows that similar to TS1, for this stage the positions and numbers of HBs are similar for two substrates in hydrolysis and perhydrolysis reactions. This structural similarity makes energy barriers, Table 2 and Fig. 6, identical for two substrates. As well as, the second activation energies of hydrolysis and perhydrolysis reactions are similar. In fact, the absence of the intermolecular HB in the TS2 structures of perhydrolysis reaction, which is obvious from Fig. 9 and Table 1, causes this likeness. The same trend is distinguished for the second free activation energies. As Fig. 6 and Table 2 display, the free energy barriers of the second stage of hydrolysis and perhydrolysis reactions are almost identical.

After passing through the TS2 state and releasing the product of the reaction, the EP complexes is formed. As is shown in Fig. 10, in this step the serine residue separates from carboxylic or percarboxylic group, and the product is liberated. If the hydrolysis reaction is occurred, the product will be carboxylic acid while in the perhydrolysis reaction the proxyacid will be produce. Relative energies and free energies display that this complex is the most stable form among all the chemical species in both hydrolysis and perhydrolysis reactions. Stability of EP complex alters from 5.8 to 9.6 kcal mol^{-1} at different computational levels. More stability of this arises from its special geometry. When the product is released, the steric hindrances on the TI structure reduce and system becomes relaxed. Also, this make possible forming HB network in catalytic triad that increases the structure stability. Based on optimized structures and their calculated topological parameters besides above causes forming HBs between product and oxyanion hole residues can result in stability (see Fig. 10 and Table 1).

3.2. Detailed evaluation of calculated relative energies

As is mentioned here we used two quantum mechanics levels for our calculations. In this part of article, we compared the earned results of these different methods and evaluated their exactness. At low-level calculations, B3PW91/6-31G(d), Cap-E deacylation by H_2O wants 11.3 kcal mol^{-1} energy to pass over the energy barrier of TS1 while this energy is 10.9 kcal mol^{-1} for deacylation of Act-E. The perhydrolysis reaction needs 9.4 and 8.7 kcal mol^{-1} energies for Cap-E and Act-E, respectively, to overcome this energy maximum. By applying the zero-point energy corrections, the significant changes do not note in the activation energies. Equally development of computational level, B3PW91/6-311++G(d,p), only decreases a few energy barriers, maximum 0.7 kcal mol^{-1}, which are not notable values.

As is said TI formation is associated with energy increasing such that in both reactions the energy of TI is higher than AE + R′OH complex. This tetrahedral intermediate needs 5.6 and 6.3 kcal mol^{-1} of energy to cross over the TS2 energy barrier and convert to EP stable structure in the hydrolysis reaction of Cap-E and Act-E at low-level. In perhydrolysis reaction the energy barriers remain almost constant, which cause of this likeness for this stage of reactions was described in the previous section. A similar scheme is distinguished for improved calculation levels. Implementation of zero-point energy corrections and increasing the calculation level do not have important effect on the second activation energies of two reactions.

Based on these observations we can say that the obtained results at low computational level are valid and can be used without increasing the cost of calculations. So the relative Gibbs free energies of two reactions, which are gained by using the frequency calculations in the low-level of theory, are used for pathway investigation from the free energy viewpoint. As is obvious the changes trend of free energies are similar to relative energy changes. In the hydrolysis reaction, the Cap-E and Act-E structures employ 10.5 and 10.0 kcal mol^{-1} free energies to overpower the first energy barrier whereas this lessens to 5.9 and 5.6 kcal mol^{-1} for the second activation energies, respectively (Fig. 6 and Table 2). These values of free energies are comparable with energies that were reported for the deacylation step of AChE and BuChE hydrolysis with ACh. In the computational studies that were done by Yanzi Zhou [1] and Xi Chen [30] the calculated free energy barriers for passing from first transition state are almost between 10.8 to 17.5 kcal mol^{-1}. These papers reported the 2.0 to 6.9 kcal mol^{-1} free energy barriers for the second transition state. Comparison of our results with these reported values tell us that the hydrolysis of Cap-E and Act-E could theoretically be done. For perhydrolysis reaction, these free energy values become 8.3 and 8.1 kcal mol^{-1} for the first and 5.0 and 4.7 kcal mol^{-1} for the second activation energies. These reported values are also in the acceptable range and confirm the possibility of perhydrolysis reaction in theory.

Finally comparison of acylation [31] and deacylation free energy barriers shows that the rate determining step are different for two substrates. In hydrolysis and perhydrolysis of MEC, the deacylation step control the rate of reaction, with the higher activation energy, whereas the acylation step plays this role for ACh.

4. Conclusion

The reaction pathway of the deacylation step of methylcaprylate and acetylcholine hydrolysis and perhydrolysis reactions by Lipase B was studied by DFT methods starting from an experimentally mechanism was suggested before. Five different species including the AE + R′OH, TS, TI and EP structures along the two reaction paths were identified and examined by two levels of theories. The density of bond critical point explored the type and strength of interactions, which were reached by using AIM tools.

Energy and free energy pathways of two reactions were reported. Based on obtained results, the first step of hydrolysis reaction was occurred with fewer energy in acetyl-enzyme with respect to capryloyl-enzyme. The perhydrolysis reactions were going through a similar process with little loss in energy values and as the hydrolysis reaction, the first activation energy of acetyl-enzyme is fewer than capryloyl–enzyme. Passing from second energy barrier is associated with a significantly reduced in energy values of hydrolysis and perhydrolysis reactions. In this stage of reactions, almost half of first activation energies needs to pass from energy barrier.

Comparison of acylation, our pervious article, and deacylation energy barriers shows that the rate determining step are different for two substrates. In hydrolysis and perhydrolysis of MEC, the deacylation step control the rate of reaction, with the higher activation energy, whereas the acylation step plays this role for ACh. This minimized energy profiles shows that the reaction pathway of hydrolysis and perhydrolysis of ACh, its transition states and intermediates are confirmable. Comparison with reported data of similar reactions suggested that this reaction might be theoretically probable.

Acknowledgment

This research was supported by Ferdowsi University of Mashhad, Iran (grant 3/20408-07 March 2012).

Appendix A. Supplementary data

Supplementary data associated with this article can be found, in the online version, at http://dx.doi.org/10.1016/j.jmgm.2015.01.003.

References

[1] Y. Zhou, S. Wang, Y. Zhang, Catalytic reaction mechanism of acetylcholinesterase determined by Born–Oppenheimer ab initio QM/MM molecular dynamics simulations, J. Phys. Chem. B 114 (2010) 8817–8825.
[2] P.A. Frey, A.D. Hegeman, Enzymatic Reaction Mechanisms, Oxford University Press, Oxford, 2007.
[3] D.A. Kraut, K.S. Carroll, D. Herschlag, Challenges in enzyme mechanism and energetics, Annu. Rev. Biochem. 72 (2003) 517–571.
[4] M.H. Potashman, M.E. Duggan, Covalent modifiers: an orthogonal approach to drug design, J. Med. Chem. 52 (2009) 1231–1246.
[5] V.L. Schramm, Enzymatic transition state theory and transition state analogue design, J. Biol. Chem. 282 (2007) 28297–28300.
[6] V. Nanda, R.L. Koder, Designing artificial enzymes by intuition and computation, Nat. Chem. 2 (2010) 15–24.
[7] M. Roca, A. Vardi-Kilshtain, A. Warshel, Toward accurate screening in computer-aided enzyme design, Biochemistry 48 (2009) 3046–3056.
[8] E.B. De Oliveira, C. Humeau, E.R. Maia, L. Chebil, E. Ronat, G. Monard, et al., An approach based on density functional theory (DFT) calculations to assess the *Candida antarctica* lipase B selectivity in rutin, isoquercitrin and quercetin acetylation, J. Mol. Catal. B: Enzym. 66 (2010) 325–331.
[9] M. Svedendahl, P. Carlqvist, C. Branneby, O. Allnér, A. Frise, K. Hult, et al., Direct epoxidation in *Candida antarctica* lipase B studied by experiment and theory, ChemBioChem 9 (2008) 2443–2451.
[10] P. Braiuca, K. Lorena, V. Ferrario, C. Ebert, L. Gardossi, A three-dimensional quanititative structure–activity relationship (3D-QSAR) model for predicting the enantioselectivity of *Candida antarctica* lipase B, Adv. Synth. Catal. 351 (2009) 1293–1302.
[11] M. Nardini, B.W. Dijkstra, α/β Hydrolase fold enzymes: the family keeps growing, Curr. Opin. Struct. Biol. 9 (1999) 732–737.
[12] Z.S. Derewenda, A.M. Sharp, News from the interface: the molecular structures of triacyglyceride lipases, Trends Biochem. Sci. 18 (1993) 20–25.
[13] Mohammad Sadegh Sadeghi Googheri, Mohammad Reza Housaindokht, Hassan Sabzyan, Reaction mechanism and free energy profile for acylation of *Candida antarctica* lipase, B. with methylcaprylate and acetylcholine; density functional theory, calculations, J. Mol. Graph. Modell. 54 (2014) 131–140.
[14] C. Li, T. Tan, H. Zhang, W. Feng, Analysis of the conformational stability and activity of *Candida antarctica* lipase B in organic solvents, J. Biol. Chem. 285 (2010) 28434–28441.
[15] A. Houde, A. Kademi, D. Leblanc, Lipases and their industrial applications: an overview, Appl. Biochem. Biotechnol. 118 (2004) 155–170.
[16] M. Martinelle, K. Hult, Kinetics of acyl transfer reactions in organic media catalysed by *Candida antarctica* lipase B, Biochim. Biophys. Acta 1251 (1995) 191–197.
[17] J. Kraut, Serine proteases: structure and mechanism of catalysis, Annu. Rev. Biochem. 46 (1977) 331–358.
[18] K. Kim, O.G. Tsay, D.A. Atwood, D.G. Churchill, Destruction and detection of chemical warfare agents, Chem. Rev. 111 (2011) 5345–5403.
[19] R.F.W. Bader, Atoms in Molecules: A Quantum Theory, Oxford University Press, Oxford, 1994 (Incorporated).
[20] A.D. Becke, Density-functional thermochemistry, III. The role of exact exchange, J. Chem. Phys. 98 (1993) 5648–5652.
[21] P. Ziesche, H. Eschrig (Eds.), Electronic Structure of Solids '91: Proceedings of the 75, Akademie Verlag, Berlin, 1991.

[22] J.P. Perdew, in: P. Ziesche, H. Eschrig (Eds.), Proceedings of the 75. WE-Heraeus-Seminar and 21st Annual International Symposium on Electronic Structure of Solids, March 11–15, 1991, Gaussig, Germany, 1991, pp. 11–20.
[23] A.K. Rappe, C.J. Casewit, K.S. Colwell, W.A. Goddard, W.M. Skiff, UFF, a full periodic table force field for molecular mechanics and molecular dynamics simulations, J. Am. Chem. Soc. 114 (1992) 10024–10035.
[24] V. Barone, M. Cossi, Quantum calculation of molecular energies and energy gradients in solution by a conductor solvent model, J. Phys. Chem. A 102 (1998) 1995–2001.
[25] M. Cossi, N. Rega, G. Scalmani, V. Barone, Energies, structures, and electronic properties of molecules in solution with the C-PCM solvation model, J. Comput. Chem. 24 (2003) 669–681.
[26] M.J. Frisch, G.W. Trucks, H.B. Schlegel, G.E. Scuseria, M.A. Robb, J.R. Cheeseman, et al., Gaussian 09, Revision B.01, Gaussian, Inc, Wallingford, CT, 2009.
[27] T. Keith, AIMAll 10.05.04, TK Gristmill Software, 2010.
[28] S. Jenkins, Z. Liu, S.R. Kirk, A bond, ring and cage resolved Poincaré–Hopf relationship for isomerisation reaction pathways, Mol. Phys. 111 (2013) 3104–3116.
[29] C. Peng, P.Y. Ayala, H.B. Schlegel, M.J. Frisch, Using redundant internal coordinates to optimize equilibrium geometries and transition states, J. Comput. Chem. 17 (1996) 49–56.
[30] X. Chen, L. Fang, J. Liu, C.-G. Zhan, Reaction pathway and free energy profile for butyrylcholinesterase-catalyzed hydrolysis of acetylcholine, J. Phys. Chem. B 115 (2010) 1315–1322.
[31] M.S. Sadeghi Googheri, M.R. Housaindokht, H. Sabzyan, Reaction mechanism and free energy profile for acylation of *Candida Antarctica* lipase B with methyl-caprylate and acetylcholine: density functional theory calculations, J. Mol. Graph. Modell. 54 (2014) 131–140.